

## Research paper

# An unconditionally stable second-order accurate method for systems of Cahn–Hilliard equations



Junxiang Yang, Junseok Kim\*

Department of Mathematics, Korea University, Seoul, 02841, Republic of Korea

## ARTICLE INFO

## Article history:

Received 29 November 2019

Revised 8 March 2020

Accepted 23 March 2020

Available online 31 March 2020

## Keywords:

Systems of Cahn–Hilliard equations

second-order accuracy

unconditionally stable scheme

finite difference method

## ABSTRACT

In this paper, we develop an unconditionally stable linear numerical scheme for the  $N$ -component Cahn–Hilliard system with second-order accuracy in time and space. The proposed scheme is modified from the Crank–Nicolson finite difference scheme and adopts the idea of a stabilized method. Nonlinear multigrid algorithm with Gauss–Seidel-type iteration is used to solve the resulting discrete system. We theoretically prove that the proposed scheme is unconditionally stable for the whole system. The numerical solutions show that the larger time steps can be used and the second-order accuracy is obtained in time and space; and they are consistent with the results of linear stability analysis. We investigate the evolutions of triple junction and spinodal decomposition in a quaternary mixture. Moreover, the proposed scheme can be modified to solve the binary spinodal decomposition in complex domains and multi-component fluid flows.

© 2020 Elsevier B.V. All rights reserved.

## 1. Introduction

The Cahn–Hilliard (CH) equation is an important fourth-order nonlinear partial differential equation in phase-field method. It was originally derived from the work of Cahn and Hilliard [1] to model the binary alloy evolution. By taking some modifications, the classical CH equation can be extended to model the two-phase fluid flow [2,3], vesicle membrane [4], tumor growth [5,6], diblock copolymer [7], surface smoothing [8], and structural optimization [9], etc., see [10] for the various applications of the CH equation. However, the classical CH equation with arbitrary initial condition does not have analytical solution and it also brings some challenges in numerical computations because the existence of nonlinear part and second-order derivative of Laplacian operator. Therefore, the simplest explicit Euler method is very inefficient for the calculation of the CH equation. Naturally, accurate and efficient fully implicit or semi-implicit numerical schemes should be developed for the CH equation.

The CH equation has two important physical properties: the total mass conservation and total energy dissipation. Therefore, we want the numerical schemes can still satisfy the discrete forms of mass conservation and energy dissipation under any time step size. Kim et al. [11] developed a conservative multigrid algorithm for the CH system, where the second-order Crank–Nicolson (CN) scheme was adopted. However, the CN scheme is not strictly unconditionally stable if a large time step is used. Eyre [12] developed the convex splitting scheme for the CH equation and the Allen–Cahn (AC) equation. Jeong et al. [13] adopted the complex splitting method to verify a new benchmark problem for the CH model. Based on the convex

\* Corresponding author.

E-mail address: [cfdkim@korea.ac.kr](mailto:cfdkim@korea.ac.kr) (J. Kim).URL: <http://math.korea.ac.kr/~cfdkim> (J. Kim)

splitting scheme, Lee and Shin [14] developed an unconditionally stable compact scheme for the CH equation. Note that the convex splitting method has the merits of unconditional stability and unique solvability under any time step size, however it is generally first-order accurate in time. Later, a stabilized method was developed in [15] to achieve unconditional stability. However, the general stabilized method only has first-order accuracy in time. Zhao et al. [16] numerically investigated the power law scaling dynamics of the CH equations with various mobilities, where a stabilizing constant is used to keep energy stability. Comparing with the first-order schemes, second-order time accurate schemes are more popular in recent years. A popular method for constructing unconditionally stable, second-order time accurate schemes is based on the CN approach. Chen et al. [17] proposed a second-order energy stable scheme for the Cahn–Hilliard–Hele–Shaw (CHHS) models. Diegel et al. [18] performed the convergence and error analysis of a CN-type second-order scheme for the Cahn–Hilliard–Navier–Stokes (CHNS) system. Another popular method is to use the second-order backward difference formula (BDF2) for temporal discretization. Yan et al. [19] developed a second-order temporal accurate method for the CH equation based on the BDF2 scheme. Chen et al. [20] constructed second-order, energy stable, and positivity-preserving schemes for the CH model with logarithmic potential. Cheng et al. [21] constructed a fourth-order finite difference scheme for the CH equation, where the second-order time accuracy is achieved by using a BDF2 stencil. The pseudo-spectral method is also a practical and efficient technique to develop second-order and energy stable schemes for the phase-field models, please see [22,23] for some details. Recently, the second-order mixed finite element method has extensive applications for the CH model. Diegel et al. [24] investigated the stability and convergence of the mixed finite element method for the CH equation. Brenner et al. [25] proposed a robust numerical solver for the second-order mixed finite element method. Diegel et al. [26] investigated the second-order mixed finite element method for the Cahn–Hilliard–Darcy–Stokes (CHDS) system. Furthermore, Weng et al. [27] developed a high-order Fourier spectral for the space fractional CH equation with high efficiency. Guillén-González and Tierra [28] proposed a Lagrange multiplier approach for the CH equation, which can easily achieve second-order accuracy in time. Later, Yang et al. [29] improved the Lagrange multiplier approach and developed the well-known invariant energy quadratization (IEQ) approach for various gradient flow problems. Shen et al. [30] further improved the IEQ approach and proposed the scalar auxiliary variable (SAV) approach. Zhu et al. [31] extended the SAV method to the hydrodynamics coupled phase-field model. Note that the Lagrange multiplier, IEQ, and SAV approaches all can be used to easily construct second-order schemes for the CH equation. In a new work of Li et al. [32], a second-order linear scheme was constructed based on the CN scheme and stabilized method. Besides that, the approaches based on the Runge–Kutta (RK) type method have been also studied by some researchers [33,34]. Up to now, the numerical schemes mentioned above are designed for the binary CH equation. In some physical problems, the system is usually multi-component, i.e., more than two phases. Some typical examples are the multi-phase alloys [35], the multi-component fluid flow [36,37], and the ternary nanowires [38]. Therefore, it is important to construct accurate and practical numerical schemes for the multi-component (or  $N$ -component) CH system. Lee and Kim [39] constructed an accurate second-order scheme for the  $N$ -component CH system, however their method is not unconditionally stable. Later, Lee et al. [40] developed an unconditionally stable-type scheme for the  $N$ -component CH system, which is based on the first-order convex splitting method. In fact, there are few studies of the second-order accurate and unconditionally stable method for the  $N$ -component CH system. Actually, the unconditional stability is hard to prove for the  $N$ -component CH system because the existence of nonlinear source term. Note that both of the IEQ [41] and the SAV [30] can be extended to the multi-component CH system, however their approaches need to solve a  $3 \times 3$  system because the auxiliary variables are used. That costs extra computational time. Here, we develop an unconditionally stable numerical method for the  $N$ -component CH system with second-order accuracy in time and space. The proposed scheme is derived from the CN scheme and adopts the idea of stabilized method. The proposed scheme is proved to be unconditionally stable for the whole system. Moreover, our scheme is easy to implement because all nonlinear terms are treated to be the source terms.

In Section 2, we present the governing equation of the  $N$ -component CH system and show its basic properties, i.e., the mass conservation and the energy dissipation. In Section 3, we describe the proposed numerical method. A proof of unconditional stability is given in Section 4. Section 5 presents various numerical experiments. Conclusions are derived in Section 6.

## 2. Governing equations

We consider a system which consists of  $N$  components in a domain  $\Omega$ . Let  $c_k = c_k(\mathbf{x}, t)$  be the mole fraction of the  $i$ th phase variable, which is the function of space  $\mathbf{x}$  and time  $t$ . It is obvious that the summation of  $c_k$  is 1, i.e.,

$$c_1 + c_2 + \dots + c_N = 1. \quad (1)$$

Let  $\mathbf{c} = (c_1, c_2, \dots, c_N)$  be the vector phase variables, then  $\mathbf{c} \in G_s$ , which is Gibbs  $N$ -simplex:

$$G_s = \left\{ \mathbf{c} \in \mathbb{R}^N \mid \sum_{k=1}^N c_k = 1, \quad 0 \leq c_k \leq 1 \text{ for } k = 1, 2, \dots, N \right\}. \quad (2)$$

Without loss of generality, we consider the following total free energy functional:

$$\mathcal{E}(\mathbf{c}) = \int_{\Omega} \left( \sum_{k=1}^N F(c_k) + \frac{\epsilon^2}{2} \sum_{k=1}^N |\nabla c_k|^2 \right) d\mathbf{x}, \quad (3)$$

where  $F(c_k)$  is a truncated potential functional. We constrict the growth of  $F(c_k)$  to be quadratic for  $c_k \geq 1.25$  or  $c_k \leq -0.25$ , i.e., the following truncated potential is used for  $k = 1, 2, \dots, N$ :

$$F(c_k) = \begin{cases} 0.7188c_k^2 + 0.125c_k + 0.0107 & \text{if } c_k \leq -0.25, \\ 0.25c_k^2(c_k - 1)^2 & \text{if } -0.25 < c_k < 1.25, \\ 0.7188c_k^2 - 1.5625c_k + 0.8545 & \text{if } c_k \geq 1.25. \end{cases} \tag{4}$$

$\epsilon$  is a positive parameter related to the interfacial energy. The temporal evolution of each component  $c_k$  is governed by the following multi-component CH system:

$$\frac{\partial c_k}{\partial t} = \Delta \mu_k, \tag{5}$$

$$\mu_k = F'(c_k) - \epsilon^2 \Delta c_k + \beta(\mathbf{c}), \text{ for } k = 1, 2, \dots, N, \tag{6}$$

where  $\mu$  is the chemical potential,  $F'(c_k) = c_k(c_k - 0.5)(c_k - 1)$ ,  $\beta(\mathbf{c}) = -\frac{1}{N} \sum_{k=1}^N F'(c_k)$  is a variable Lagrangian multiplier which is used to satisfy the mass conservative constraint in Eq. (1). To achieve the mass conservation of the whole system, the zero Neumann boundary condition is used for each  $\mu_k$ :

$$\nabla \mu_k \cdot \mathbf{n} = 0 \text{ on } \partial\Omega. \tag{7}$$

Here,  $\mathbf{n}$  is the unit normal vector to the domain boundary  $\partial\Omega$ . We differentiate the total energy  $\mathcal{E}(\mathbf{c})$  and the total mass of each component  $\int_{\Omega} c_k \mathbf{d}\mathbf{x}$  with respect to time  $t$

$$\begin{aligned} \frac{d}{dt} \mathcal{E}(\mathbf{c}) &= \int_{\Omega} \sum_{k=1}^N \left( \frac{\partial F(\mathbf{c})}{\partial t} \frac{\partial c_k}{\partial t} + \epsilon^2 \nabla c_k \cdot \nabla \frac{\partial c_k}{\partial t} \right) \mathbf{d}\mathbf{x} \\ &= \int_{\Omega} \sum_{k=1}^N \frac{\partial F(\mathbf{c})}{\partial t} \frac{\partial c_k}{\partial t} \mathbf{d}\mathbf{x} + \int_{\partial\Omega} \sum_{k=1}^N \epsilon^2 \nabla c_k \cdot \mathbf{n} \frac{\partial c_k}{\partial t} ds - \int_{\Omega} \sum_{k=1}^N \epsilon^2 \Delta c_k \frac{\partial c_k}{\partial t} \mathbf{d}\mathbf{x} \\ &= \int_{\Omega} \sum_{k=1}^N \left( \frac{\partial F(\mathbf{c})}{\partial c_k} - \epsilon^2 \Delta c_k \right) \frac{\partial c_k}{\partial t} \mathbf{d}\mathbf{x} = \int_{\Omega} \sum_{k=1}^N (\mu_k - \beta(\mathbf{c})) \frac{\partial c_k}{\partial t} \mathbf{d}\mathbf{x} \\ &= \int_{\Omega} \sum_{k=1}^N \mu_k \Delta \mu_k \mathbf{d}\mathbf{x} - \beta(\mathbf{c}) \int_{\Omega} \sum_{k=1}^N \frac{\partial c_k}{\partial t} \mathbf{d}\mathbf{x} = - \int_{\Omega} \sum_{k=1}^N |\nabla \mu_k|^2 \mathbf{d}\mathbf{x} \leq 0 \end{aligned} \tag{8}$$

and

$$\frac{d}{dt} \int_{\Omega} c_k \mathbf{d}\mathbf{x} = \int_{\Omega} \frac{\partial c_k}{\partial t} \mathbf{d}\mathbf{x} = \int_{\Omega} \Delta \mu_k \mathbf{d}\mathbf{x} = \int_{\partial\Omega} \nabla \mu_k \cdot \mathbf{n} ds = 0, \tag{9}$$

where the homogenous Neumann boundary condition in Eq. (7) is used. Obviously, we can find that the total energy of the whole system is non-increasing and the total mass of each component is conservative in time.

### 3. Numerical solution

We describe the proposed numerical scheme in two-dimensional space  $\Omega = (a, b) \times (c, d)$ , the extension to three-dimensional space is straightforward. We only need to solve the  $N - 1$  components successively, the  $N$ th component can be naturally obtained by  $c_N = 1 - c_1 - c_2 \dots - c_{N-1}$ . Let  $N_x$  and  $N_y$  be the positive even mesh sizes in  $x$ - and  $y$ -directions, respectively. The uniform space step is defined to be  $h = (b - a)/N_x = (d - c)/N_y$ . The set of cell-centers is defined as  $\Omega_d = \{(x_i, y_j) : x_i = a + (i - 0.5)h, y_j = c + (j - 0.5)h, 1 \leq i \leq N_x, 1 \leq j \leq N_y\}$ . The time step is defined to be  $\Delta t = T/N_t$ , where  $T$  is the total computational time,  $N_t$  is the number of temporal evolution. We define  $c_{k,ij}$  and  $\mu_{k,ij}$  be the approximations of  $c_k(x_i, y_j)$  and  $\mu_k(x_i, y_j)$ , respectively. In the previous work of Lee and Kim [39], the following Crank–Nicolson scheme was used for the  $N$ -component CH system to achieve second-order accuracy in time

$$\frac{c_{k,ij}^{n+1} - c_{k,ij}^n}{\Delta t} = \Delta_d \mu_{k,ij}^{n+\frac{1}{2}}, \tag{10}$$

$$\mu_{k,ij}^{n+\frac{1}{2}} = \frac{1}{2} (F'(c_{k,ij}^{n+1}) + F'(c_{k,ij}^n)) - \frac{\epsilon^2}{2} (\Delta_d c_{k,ij}^{n+1} + \Delta_d c_{k,ij}^n) + \frac{1}{2} (\beta(\mathbf{c}_{ij}^{n+1}) + \beta(\mathbf{c}_{ij}^n)), \text{ for } k = 1, 2, \dots, N, \tag{11}$$

where the discrete five-point Laplacian operator is  $\Delta_d \phi_{ij} = (\phi_{i+1,j} + \phi_{i-1,j} + \phi_{i,j+1} + \phi_{i,j-1} - 4\phi_{ij})/h^2$ . Although the CN scheme has second-order accuracy in time, it is hard to satisfy the energy law because of the existence of nonlinear term  $F'(c_k)$ . To develop a second order scheme that does satisfy an energy law, we adopt the idea of stabilized method to divide

the nonlinear term at  $n + 1$  time level  $F'(c_k^{n+1})$  into two parts:  $F'(c_k^{n+1}) - \gamma c_k^{n+1}$  and  $\gamma c_k^{n+1}$ . To avoid solving the nonlinear system, we approximate  $F'(c_k^{n+1}) - \gamma c_k^{n+1}$  by using the second-order accurate extrapolation from previous values, i.e.,  $F'(c_k^{n+1}) - \gamma c_k^{n+1} \approx 2(F'(c_k^n) - \gamma c_k^n) - (F'(c_k^{n-1}) - \gamma c_k^{n-1})$ . Here,  $\gamma$  is a positive stabilizing parameter. Similarly, we approximate  $\beta(c_k^{n+1})$  by  $\beta(c_k^{n+1}) \approx 2\beta(c_k^n) - \beta(c_k^{n-1})$ . Thus, the proposed second-order scheme can be written as:

$$\frac{c_{k,ij}^{n+1} - c_{k,ij}^n}{\Delta t} = \Delta_d \mu_{k,ij}^{n+\frac{1}{2}}, \tag{12}$$

$$\begin{aligned} \mu_{k,ij}^{n+\frac{1}{2}} &= \frac{3}{2}(F'(c_{k,ij}^n) - \gamma c_{k,ij}^n) - \frac{1}{2}(F'(c_{k,ij}^{n-1}) - \gamma c_{k,ij}^{n-1}) \\ &\quad + \frac{\gamma}{2}(c_{k,ij}^{n+1} + c_{k,ij}^n) - \frac{\epsilon^2}{2}(\Delta_d c_{k,ij}^{n+1} + \Delta_d c_{k,ij}^n) \\ &\quad + \frac{3}{2}\beta(c_{ij}^n) - \frac{1}{2}\beta(c_{ij}^{n-1}), \text{ for } k = 1, 2, \dots, N. \end{aligned} \tag{13}$$

To solve the resulting discrete system of Eqs. (12) and (13), we use a multigrid algorithm with Gauss–Seidel-type smoothing operator. For some details of multigrid algorithm, see [11,42,43]. Note that the proposed scheme is unconditionally stable for the whole system. A detailed proof will be presented in Section 4.

### 4. Analyses for the whole system

#### 4.1. Unconditionally stability

We prove that the proposed numerical scheme in Section 3 is unconditionally stable for the whole system. First, the discrete inner product for  $(\phi, \varphi)_d$  is defined to be

$$(\phi, \varphi)_d = h^2 \sum_{i=1}^{N_x} \sum_{j=1}^{N_y} \phi_{ij} \varphi_{ij}. \tag{14}$$

Next, the discrete inner product for  $\langle \nabla_d \phi, \nabla_d \varphi \rangle_d$  is defined by

$$\begin{aligned} \langle \nabla_d \phi, \nabla_d \varphi \rangle_d &= h^2 \left( \sum_{i=1}^{N_x-1} \sum_{j=1}^{N_y} D_x \phi_{i+\frac{1}{2},j} D_x \varphi_{i+\frac{1}{2},j} + \sum_{i=1}^{N_x} \sum_{j=1}^{N_y-1} D_y \phi_{i,j+\frac{1}{2}} D_y \varphi_{i,j+\frac{1}{2}} \right) \\ &\quad + \frac{h^2}{2} \sum_{j=1}^{N_y} D_x \phi_{\frac{1}{2},j} D_x \varphi_{\frac{1}{2},j} + \frac{h^2}{2} \sum_{j=1}^{N_y} D_x \phi_{N_x+\frac{1}{2},j} D_x \varphi_{N_x+\frac{1}{2},j} \\ &\quad + \frac{h^2}{2} \sum_{i=1}^{N_x} D_y \phi_{i,\frac{1}{2}} D_y \varphi_{i,\frac{1}{2}} + \frac{h^2}{2} \sum_{i=1}^{N_x} D_y \phi_{i,N_y+\frac{1}{2}} D_y \varphi_{i,N_y+\frac{1}{2}}, \end{aligned} \tag{15}$$

where  $D_x \phi_{i+\frac{1}{2},j}$  and  $D_y \phi_{i,j+\frac{1}{2}}$  are defined by

$$D_x \phi_{i+\frac{1}{2},j} = \frac{1}{h}(\phi_{i+1,j} - \phi_{ij}), \quad D_y \phi_{i,j+\frac{1}{2}} = \frac{1}{h}(\phi_{i,j+1} - \phi_{ij}). \tag{16}$$

The discrete zero Neumann boundary conditions are written as  $D_x \phi_{\frac{1}{2},j} = D_x \phi_{N_x+\frac{1}{2},j} = D_y \phi_{i,\frac{1}{2}} = D_y \phi_{i,N_y+\frac{1}{2}} = 0$ . Because the following proof only needs the temporal index, we omit the spatial index for convenience. We then define the discrete norm as  $\|c_k\|_d^2 = (c_k, c_k)_d$  and  $\|\nabla_d c_k\|_d^2 = \langle \nabla_d c_k, \nabla_d c_k \rangle_d$ . The discrete total energy functional of the whole system is defined to be

$$\mathcal{E}^d(c^n) = \sum_{k=1}^N \mathcal{E}^d(c_k^n), \tag{17}$$

where the discrete total energy functional of the component  $c_k$  is defined to be

$$\mathcal{E}^d(c_k^n) = (F(c_k^n), \mathbf{1})_d + \frac{\epsilon^2}{2} \langle \nabla_d c_k^n, \nabla_d c_k^n \rangle_d. \tag{18}$$

Here,  $\mathbf{1}$  is the all-ones vector. Let the discrete pseudo energy of the component  $c_k$  be

$$\tilde{\mathcal{E}}^d(c_k^{n+1}, c_k^n) = \mathcal{E}^d(c_k^{n+1}) + \frac{1}{4} [\gamma - (F''(\bar{q}^{n-1}) + 2F''(\bar{\psi}^n))] \|c_k^{n+1} - c_k^n\|_d^2, \tag{19}$$

where  $\bar{q}^{n-1}$  is a constant for the mean value theorem and will be defined in Eq. (28); and  $\bar{\psi}^n$  is a constant satisfying

$$(F'(c_k^n), c_k^{n+1} - c_k^n)_d = (F(c_k^{n+1}) - F(c_k^n), \mathbf{1})_d - \frac{1}{2} F''(\bar{\psi}^n) \|c_k^{n+1} - c_k^n\|_d^2. \tag{20}$$

Next, we start to prove that the proposed scheme (12) and (13) are unconditionally stable, i.e., the discrete total energy of the whole system is non-increasing in time under the condition  $\gamma > 3F''(M_p) \geq \max\{F''(\bar{q}^{n-1}) + 2F''(\bar{\psi}^n)\}$ , where  $\gamma$  is a positive parameter. Because the truncated potential functional in Section 2 is used. Therefore, we can define the maximum value of  $F''(c_k)$  as  $\max\{F''(c_k)\} = 3 \max\{c_k\}^2 - 3 \max\{c_k\} + 0.5$  in the computation, where  $\max\{c_k\} = M_p$  is the maximum value of  $c_k$ .

**Remark.** In this work, we follow the ideas of the stabilized method [44], where the assumption  $\|F''\|_\infty \leq L$  is satisfied by using a proper truncated potential functional, i.e., the classical double-well potential  $F$  is restricted to quadratic for  $c_k \geq M_p$  or  $c_k \leq 1 - M_p$ . Here  $M_p$  is a constant and  $M_p \geq 1$ . Using this assumption, the classical stabilized method can be proved to be unconditionally stable. The main reason for this approach is that many physically relevant researches focus on the results locating in  $0 \leq c_k \leq 1$ . Please refer to [45,46] for some applications of truncated potential functional of the CH model. Because the truncated potential functional in Section 2 is used. Thus, we can easily find the maximum value of  $F''$ .

**Lemma 1.** Three solutions  $(c_k^{n+1}, c_k^n, c_k^{n-1})$  of the scheme (12) and (13) satisfy:

$$\mathcal{E}^d(c_k^{n+1}) \leq \tilde{\mathcal{E}}^d(c_k^{n+1}, c_k^n). \tag{21}$$

**Proof.** Eq. (18) subtracts Eq. (19), we have

$$\mathcal{E}^d(c_k^{n+1}) - \tilde{\mathcal{E}}^d(c_k^{n+1}, c_k^n) = -\frac{1}{4}[\gamma - (F''(\bar{q}^{n-1}) + 2F''(\bar{\psi}^n))] \|c_k^{n+1} - c_k^n\|_d^2 \leq 0. \tag{22}$$

Here, the condition  $\gamma > 3F''(M_p) \geq \max\{F''(\bar{q}^{n-1}) + 2F''(\bar{\psi}^n)\}$  is used.  $\square$

**Theorem 1.** If  $c_k^{n+1}$ ,  $c_k^n$ , and  $c_k^{n-1}$  are the solutions of Eqs. (12) and (13), then the following energy law of the whole system holds for any time step  $\Delta t$ :

$$\tilde{\mathcal{E}}^d(\mathbf{c}^{n+1}, \mathbf{c}^n) \leq \tilde{\mathcal{E}}^d(\mathbf{c}^n, \mathbf{c}^{n-1}). \tag{23}$$

**Proof.** We multiply Eq. (12) by  $\mu_k^{n+\frac{1}{2}}$  and then take the discrete inner product, we have

$$\begin{aligned} (c_k^{n+1} - c_k^n, \mu_k^{n+\frac{1}{2}})_d &= \Delta t (\Delta_d \mu_k^{n+\frac{1}{2}}, \mu_k^{n+\frac{1}{2}})_d \\ &= -\Delta t (\nabla_d \mu_k^{n+\frac{1}{2}}, \nabla_d \mu_k^{n+\frac{1}{2}})_d \\ &= -\Delta t \|\nabla_d \mu_k^{n+\frac{1}{2}}\|_d^2. \end{aligned} \tag{24}$$

We multiply Eq. (13) by  $c_k^{n+1} - c_k^n$  and take the discrete inner product by parts, we have

$$-\left(\frac{\epsilon^2}{2} \Delta_d c_k^{n+1} + \frac{\epsilon^2}{2} \Delta_d c_k^n, c_k^{n+1} - c_k^n\right)_d = \frac{\epsilon^2}{2} \|\nabla_d c_k^{n+1}\|_d^2 - \frac{\epsilon^2}{2} \|\nabla_d c_k^n\|_d^2, \tag{25}$$

$$\frac{\gamma}{2} (c_k^{n+1} - 2c_k^n + c_k^{n-1}, c_k^{n+1} - c_k^n)_d = \frac{\gamma}{4} (\|c_k^{n+1} - c_k^n\|_d^2 - \|c_k^n - c_k^{n-1}\|_d^2 + \|c_k^{n+1} - 2c_k^n + c_k^{n-1}\|_d^2), \tag{26}$$

$$\begin{aligned} (F'(c_k^n), c_k^{n+1} - c_k^n)_d &= (F(c_k^{n+1})_k - F(c_k^n), \mathbf{1})_d - \left(\frac{1}{2}F''(\bar{\psi}^n)(c_k^{n+1} - c_k^n), c_k^{n+1} - c_k^n\right)_d \\ &= (F(c_k^{n+1}) - F(c_k^n), \mathbf{1})_d - \frac{1}{2}F''(\bar{\psi}^n) \|c_k^{n+1} - c_k^n\|_d^2. \end{aligned} \tag{27}$$

Here, the Taylor expansion and mean value theorem are used in Eq. (27). Note that  $\bar{\psi}^n$  is a value locates between  $c_k^{n+1}$  and  $c_k^n$  from Taylor expansion. The constant value  $\bar{\psi}^n$  exists because of the mean value theorem. In a similar manner, we can have

$$\begin{aligned} \left(\frac{1}{2}F'(c_k^n) - \frac{1}{2}F'(c_k^{n-1}), c_k^{n-1} - c_k^n\right)_d &= \left(\frac{1}{2}F''(\bar{\psi}^{n-1})(c_k^n - c_k^{n-1}), c_k^{n+1} - c_k^n\right)_d \\ &= \left(\frac{1}{2}F''(\bar{\psi}^{n-1})(c_k^n - c_k^{n-1}), c_k^n - c_k^{n-1}\right)_d + \left(\frac{1}{2}F''(\bar{\psi}^{n-1})(c_k^{n+1} - 2c_k^n + c_k^{n-1}), c_k^n - c_k^{n-1}\right)_d \\ &= \frac{1}{2}F''(\bar{\psi}^{n-1})(c_k^n - c_k^{n-1}, c_k^n - c_k^{n-1})_d + \frac{1}{2}F''(\bar{q}^{n-1})(c_k^{n+1} - 2c_k^n + c_k^{n-1}, c_k^n - c_k^{n-1})_d \\ &= -\frac{F''(\bar{q}^{n-1})}{4} (\|c_k^{n+1} - c_k^n\|_d^2 - \|c_k^n - c_k^{n-1}\|_d^2 - \|c_k^{n+1} - 2c_k^n + c_k^{n-1}\|_d^2) + \frac{1}{2}F''(\bar{\psi}^{n-1}) \|c_k^n - c_k^{n-1}\|_d^2. \end{aligned} \tag{28}$$

Here,  $\bar{\psi}^{n-1}$  is constant for the Taylor expansion,  $\bar{\psi}^{n-1}$  and  $\bar{q}^{n-1}$  are the constants for the mean value theorem.

$$\left(\frac{3}{2}\beta(\mathbf{c}^n) - \frac{1}{2}\beta(\mathbf{c}^{n-1}), c_k^{n+1} - c_k^n\right)_d = \left(\frac{3}{2}\beta(\mathbf{c}^n), c_k^{n+1} - c_k^n\right)_d - \left(\frac{1}{2}\beta(\mathbf{c}^{n-1}), c_k^{n+1} - c_k^n\right)_d. \tag{29}$$

By using the definition of discrete pseudo energy in Eq. (19) and combining the Eqs. (24)-(29) together, we have

$$\begin{aligned}
 \tilde{\mathcal{E}}^d(c_k^{n+1}, c_k^n) - \tilde{\mathcal{E}}^d(c_k^n, c_k^{n-1}) &= \frac{\epsilon^2}{2} \|\nabla_d c_k^{n+1}\|_d^2 - \frac{\epsilon^2}{2} \|\nabla_d c_k^n\|_d^2 + (F(c_k^{n+1}) - F(c_k^n), \mathbf{1})_d \\
 &+ \frac{1}{4} [\gamma - (F''(\bar{Q}^{n-1}) + 2F''(\bar{\psi}^n))] \|c_k^{n+1} - c_k^n\|_d^2 \\
 &- \frac{1}{4} [\gamma - (F''(\bar{Q}^{n-1}) + 2F''(\bar{\psi}^{n-1}))] \|c_k^n - c_k^{n-1}\|_d^2 \\
 &= -\Delta t \left\| \frac{\nabla_d \mu_k^{n+1} + \nabla_d \mu_k^n}{2} \right\|_d^2 - \left( \frac{\gamma + F''(\bar{Q}^{n-1})}{4} \right) \|c_k^{n+1} - 2c_k^n + c_k^{n-1}\|_d^2 \\
 &- \left( \frac{3}{2} \beta(\mathbf{c}^n), c_k^{n+1} - c_k^n \right)_d - \left( \frac{1}{2} \beta(\mathbf{c}^{n-1}), c_k^{n+1} - c_k^n \right)_d.
 \end{aligned} \tag{30}$$

For  $k = 1, 2, \dots, N$  in the whole system, by summing Eq. (30) together and using the constraint condition in Eq. (1), we can find that

$$\begin{aligned}
 &\left( \frac{3}{2} \beta(\mathbf{c}^n), \sum_{k=1}^N (c_k^{n+1} - c_k^n) \right)_d - \left( \frac{1}{2} \beta(\mathbf{c}^{n-1}), \sum_{k=1}^N (c_k^{n+1} - c_k^n) \right)_d \\
 &= \left( \frac{3}{2} \beta(\mathbf{c}^n), (c_1^{n+1} + \dots + c_N^{n+1}) - (c_1^n + \dots + c_N^n) \right)_d - \left( \frac{1}{2} \beta(\mathbf{c}^n), (c_1^{n+1} + \dots + c_N^{n+1}) - (c_1^n + \dots + c_N^n) \right)_d \\
 &= \left( \frac{3}{2} \beta(\mathbf{c}^n), \mathbf{0} \right)_d - \left( \frac{1}{2} \beta(\mathbf{c}^n), \mathbf{0} \right)_d = 0.
 \end{aligned} \tag{31}$$

Here,  $\mathbf{0}$  is the zero vector. Thus, we have

$$\tilde{\mathcal{E}}^d(\mathbf{c}^{n+1}, \mathbf{c}^n) - \tilde{\mathcal{E}}^d(\mathbf{c}^n, \mathbf{c}^{n-1}) = -\Delta t \sum_{k=1}^N \left\| \nabla_d \mu_k^{n+\frac{1}{2}} \right\|_d^2 - \left( \frac{\gamma + F''(\bar{Q}^{n-1})}{4} \right) \sum_{k=1}^N \|c_k^{n+1} - 2c_k^n + c_k^{n-1}\|_d^2 \leq 0. \tag{32}$$

Here, the condition  $\gamma > 3F''(M_p) \geq \max\{F''(\bar{Q}^{n-1}) + 2F''(\bar{\psi}^n)\}$  is used.  $\square$

**Theorem 2.** Suppose that  $\{c_k^n, \mu_k^{n-\frac{1}{2}}\}_{n=1}^{N_t}$  for  $k = 1, 2, \dots, N$  is a sequence of solution pairs of the scheme (12) and (13) with the initial conditions  $c_k^0$  and  $c_k^{-1}$ , where  $c_k^{-1} = c_k^0 \in [0, 1]$  for  $k = 1, 2, \dots, N$ . If  $\gamma > 3F''(M_p) \geq \max\{F''(\bar{Q}^{n-1}) + 2F''(\bar{\psi}^n)\}$  is satisfied, then we obtain that

$$\mathcal{E}^d(\mathbf{c}^{n+1}) \leq \tilde{\mathcal{E}}^d(\mathbf{c}^{n+1}, \mathbf{c}^n) \leq \mathcal{E}^d(\mathbf{c}^0). \tag{33}$$

**Proof.** By Lemma 1, we have known that  $\mathcal{E}^d(c_k^{n+1}) \leq \tilde{\mathcal{E}}^d(c_k^{n+1}, c_k^n)$  for each component. Clearly, we have the conclusion that  $\mathcal{E}^d(\mathbf{c}^{n+1}) \leq \tilde{\mathcal{E}}^d(\mathbf{c}^{n+1}, \mathbf{c}^n)$  holds for the whole system. Using the Theorem 1 and the condition  $\mathbf{c}^{-1} = \mathbf{c}^0 \in [0, 1]$ , we obtain a chain of inequalities,

$$\mathcal{E}^d(\mathbf{c}^{n+1}) \leq \tilde{\mathcal{E}}^d(\mathbf{c}^{n+1}, \mathbf{c}^n) \leq \tilde{\mathcal{E}}^d(\mathbf{c}^n, \mathbf{c}^{n-1}) \leq \dots \leq \tilde{\mathcal{E}}^d(\mathbf{c}^0, \mathbf{c}^{-1}) = \mathcal{E}^d(\mathbf{c}^0). \tag{34}$$

Therefore, we get the conclusion that the discrete energy of the whole system is non-increasing in time under the bounded initial condition and a proper stabilized parameter  $\gamma$ .

We note that the proposed scheme (12) and (13) is unconditionally stable for the whole system. The numerical results in Section 5 show that the larger time steps can satisfy the property of energy dissipation.  $\square$

#### 4.2. Mass conservation

The total mass conservation for each component is another important property of the  $N$ -component CH system. To prove that the proposed scheme satisfies the mass conservation, i.e.,  $(c_k^{n+1}, \mathbf{1})_d = (c_k^n, \mathbf{1})_d$ . By taking the discrete inner product for Eq. (12), we have

$$\begin{aligned}
 (c_k^{n+1}, \mathbf{1})_d - (c_k^n, \mathbf{1})_d &= \Delta t \left( \Delta_d \mu_k^{n+\frac{1}{2}}, \mathbf{1} \right)_d \\
 &= -\Delta t \left( \nabla_d \mu_k^{n+\frac{1}{2}}, \nabla_d \mathbf{1} \right)_d = 0.
 \end{aligned} \tag{35}$$

Here, the zero Neumann boundary condition is used for  $\mu_k$ . Therefore, the mass conservation for each component is proved.

### 4.3. Unique solvability

Here, we prove that the proposed method is uniquely solvable for any time step  $\Delta t > 0$  under a proper positive parameter  $\gamma$ , where  $\gamma > 3F''(M_p) \geq \max\{F''(\bar{\varrho}^{n-1}) + 2F''(\bar{\psi}^n)\}$ . By combining the Eq. (12) and Eq. (13), the proposed scheme is rewritten to be

$$\begin{aligned} \frac{c_k^{n+1} - c_k^n}{\Delta t} = \Delta_d \left[ \frac{3}{2} (F'(c_k^n) - \gamma c_k^n) - \frac{1}{2} (F'(c_k^{n-1}) - \gamma c_k^{n-1}) \right. \\ \left. + \frac{\gamma}{2} (c_k^{n+1} + c_k^n) - \frac{\epsilon^2}{2} (\Delta_d c_k^{n+1} + \Delta_d c_k^n) \right. \\ \left. + \frac{3}{2} \beta(\mathbf{c}^n) - \frac{1}{2} \beta(\mathbf{c}^{n-1}) \right], \text{ for } k = 1, 2, \dots, N. \end{aligned} \tag{36}$$

Here, we note that the space index is omitted. Assuming that the values at  $n$  and  $n - 1$  time levels are known, then we define the following convex functional:

$$Q(c_k) = \int_{\Omega} \left[ \frac{1}{2\Delta t} |c_k|^2 + \frac{\gamma}{4} |\nabla c_k|^2 + \frac{\epsilon^2}{4} |\Delta c_k|^2 - g^{n,n-1} c_k \right] d\mathbf{x}, \tag{37}$$

where

$$g^{n,n-1} = \frac{c^n}{\Delta t} - \Delta \left[ \frac{3}{2} (F'(c_k^n) - \gamma c_k^n) - \frac{1}{2} (F'(c_k^{n-1}) - \gamma c_k^{n-1}) + \frac{\gamma}{2} c_k^n - \frac{\epsilon^2}{2} \Delta c_k^n + \frac{3}{2} \beta(\mathbf{c}^n) - \frac{1}{2} \beta(\mathbf{c}^{n-1}) \right].$$

By taking the variational derivative of  $Q(c_k)$  for  $c_k$  at  $n + 1$  time level, we obtain

$$\left. \frac{\delta Q}{\delta c_k} \right|_{c_k=c_k^{n+1}} = \frac{1}{\Delta t} c_k^{n+1} - \frac{\gamma}{2} \Delta c_k^{n+1} + \frac{\epsilon^2}{2} \Delta^2 c_k^{n+1} - g^{n,n-1}. \tag{38}$$

For a convex functional  $Q(c_k)$ , its minimum value uniquely exists as  $\frac{\delta Q}{\delta c_k} = 0$ . Therefore, we can find that the solution in the proposed scheme (36) is the minimum value of  $Q(c_k)$  in a discrete manner, that means our scheme is uniquely solvable.

## 5. Numerical results

We numerically show that the accuracy and practicability of the proposed scheme. In the simulations, the truncated potential functional in Section 2 is used. Thus, we chose a proper value  $\gamma = 5$  without specific needs. In the following tests without fluid flow, the zero Neumann boundary conditions are used for  $c_k$  and  $\mu_k$  along  $x$ - and  $y$ -directions. In the last test of multi-component fluid flow, we set the periodic boundary condition for  $c_k$  and  $\mu_k$  along  $x$ -direction and the zero Neumann boundary condition for  $c_k$  and  $\mu_k$  along  $y$ -direction.

### 5.1. Linear stability analysis

First, we investigate the short-time evolution of a four-component CH system to show the accuracy. In previous works [39,40], authors gave that the following solution of a four-component CH system:

$$\mathbf{c}(x, t) = \mathbf{m} + \sum_{k=1}^{\infty} \cos(k\pi x) (\alpha_k(t), \beta_k(t), \gamma_k(t)). \tag{39}$$

on the one-dimensional domain  $\Omega = (0, 1)$ . Here,  $\mathbf{m} = (m, m, m)$ , where  $m$  is a positive value. The evolution of  $\alpha_k(t), \beta_k(t)$ , and  $\gamma_k(t)$  are defined as:

$$\begin{aligned} (\alpha_k(t), \beta_k(t), \gamma_k(t)) = \frac{\alpha_k(0) + \beta_k(0) + \gamma_k(0)}{3} (1, 1, 1) e^{\lambda_1 t} \\ + \frac{-\alpha_k(0) - \beta_k(0) + 2\gamma_k(0)}{3} (-1, 0, 1) e^{\lambda_2 t} \\ + \frac{-\alpha_k(0) + 2\beta_k(0) - \gamma_k(0)}{3} (-1, 1, 0) e^{\lambda_3 t}, \end{aligned} \tag{40}$$

where

$$\begin{aligned} \lambda_1 &= -\frac{k^2 \pi^2}{2} (42m^2 - 15m + 1 + 2\epsilon^2 k^2 \pi^2), \\ \lambda_2 &= \lambda_3 = -\frac{k^2 \pi^2}{2} (6m^2 - 6m + 1 + 2\epsilon^2 k^2 \pi^2). \end{aligned}$$

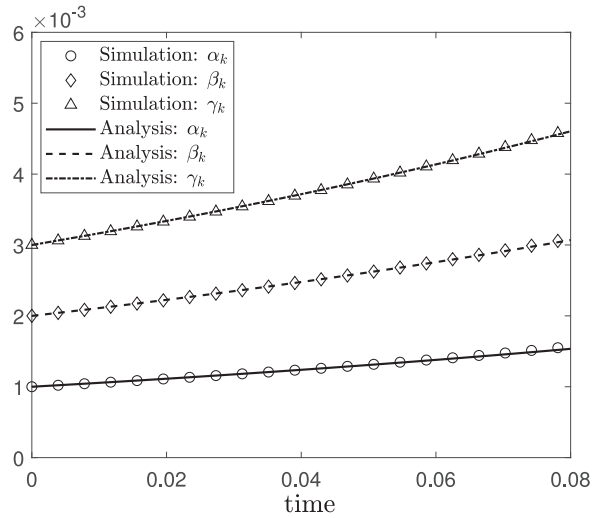


Fig. 1. Temporal evolutions of numerical and analytical values of  $\alpha_k$ ,  $\beta_k$ , and  $\gamma_k$ .

In the simulation, the initial conditions are set to be

$$c_1(x, 0) = 0.25 + 0.01 \cos(3\pi x), \quad (41)$$

$$c_2(x, 0) = 0.25 + 0.02 \cos(3\pi x), \quad (42)$$

$$c_3(x, 0) = 0.25 + 0.03 \cos(3\pi x). \quad (43)$$

The numerical parameters:  $k = 3$ ,  $m = 0.25$ ,  $h = 1/512$ ,  $\Delta t = 0.1h$ ,  $\epsilon = 0.00094$ . The numerical form of  $\alpha_k$ ,  $\beta_k$ , and  $\gamma_k$  are given as:

$$\alpha_k^n = \left( \max_{1 \leq i \leq N_x} c_1^n(x_i) - \min_{1 \leq i \leq N_x} c_1^n(x_i) \right) / 2, \quad (44)$$

$$\beta_k^n = \left( \max_{1 \leq i \leq N_x} c_2^n(x_i) - \min_{1 \leq i \leq N_x} c_2^n(x_i) \right) / 2, \quad (45)$$

$$\gamma_k^n = \left( \max_{1 \leq i \leq N_x} c_3^n(x_i) - \min_{1 \leq i \leq N_x} c_3^n(x_i) \right) / 2. \quad (46)$$

Figure 1 shows the temporal evolutions of numerical and analytical values, we can find that the numerical and analytical results are in good agreement.

## 5.2. Energy dissipation and mass conservation

The mass conservation and energy dissipation are two important properties of the  $N$ -component CH system. We numerically investigate these two properties in this part. Here, we consider the four-phase separation in two-dimensional domain  $\Omega = (0, 1)^2$ . The initial conditions are set to be

$$c_1(x, y, 0) = 0.25 + 0.1 \text{rand}(), \quad (47)$$

$$c_2(x, y, 0) = 0.25 + 0.1 \text{rand}(), \quad (48)$$

$$c_3(x, y, 0) = 0.25 + 0.1 \text{rand}(), \quad (49)$$

$$c_4(x, y, 0) = 1 - c_1(x, y, 0) - c_2(x, y, 0) - c_3(x, y, 0). \quad (50)$$

Here,  $\text{rand}()$  denotes the random number between  $-1$  and  $1$ . We use the following numerical parameters:  $h = 1/128$ ,  $\Delta t = 0.1h$ ,  $\epsilon = 0.0038$ . The discrete mass  $M^d(c_k)$  and energy  $\mathcal{E}^d(\mathbf{c})$  are defined as follows:

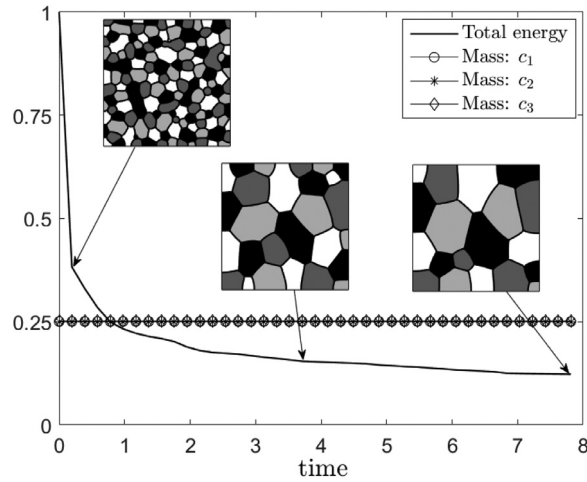


Fig. 2. Temporal evolutions of total mass and total energy. Different colors represent different components.

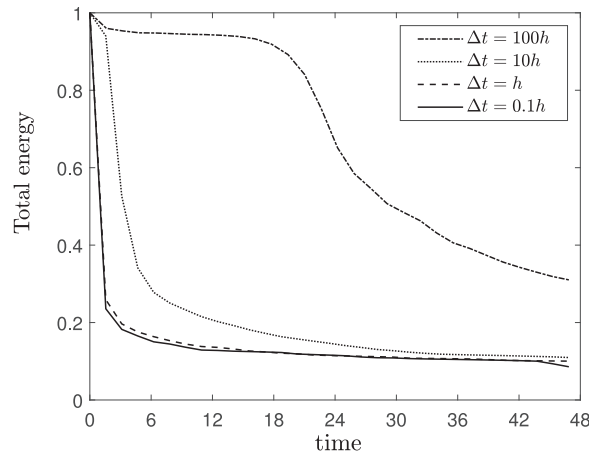


Fig. 3. Temporal evolutions of total energy with different time steps. Different colors represent different components.

$$M^d(c_k) = \frac{1}{h^2} \sum_{i=1}^{N_x} \sum_{j=1}^{N_y} c_{k,ij}, \tag{51}$$

$$\mathcal{E}^d(\mathbf{c}) = \frac{1}{h^2} \sum_{i=1}^{N_x-1} \sum_{j=1}^{N_y-1} \left[ F(\mathbf{c}_{ij}) + \frac{\epsilon^2}{2} \left( \frac{(\mathbf{c}_{i+1,j} - \mathbf{c}_{ij})^2}{h^2} + \frac{(\mathbf{c}_{i,j+1} - \mathbf{c}_{ij})^2}{h^2} \right) \right]. \tag{52}$$

The temporal evolutions of total mass and total energy are illustrated in Fig. 2, where the embedded small figures are the evolutions at particular moments. Note that the total mass and energy are both normalized by the initial values. We can find that the total mass of each component is conserved and total energy of the whole system is non-increasing in time.

### 5.3. Stability test

To verify the stability of the proposed method, we consider the four-component separation in a 2D domain  $\Omega = (0, 1)^2$ . The initial conditions and numerical parameters keep unchanged like those in Section 2. Here, a set of increasing time steps:  $\Delta t = 0.1h, h, 10h$ , and  $100h$  are used to perform the numerical experiments until  $T = 46.875$ . The temporal evolutions of discrete total energy are presented in Fig. 3. Figures 4(a), (b), (c), and (d) illustrates the final evolutions with respect to different time steps. As we can see, the total energies under different time steps are both non-increasing in time. From results in Fig. 4, we find that a large enough time step will affects the accuracy of the computation, i.e., a large enough time step makes the interfaces be rough.

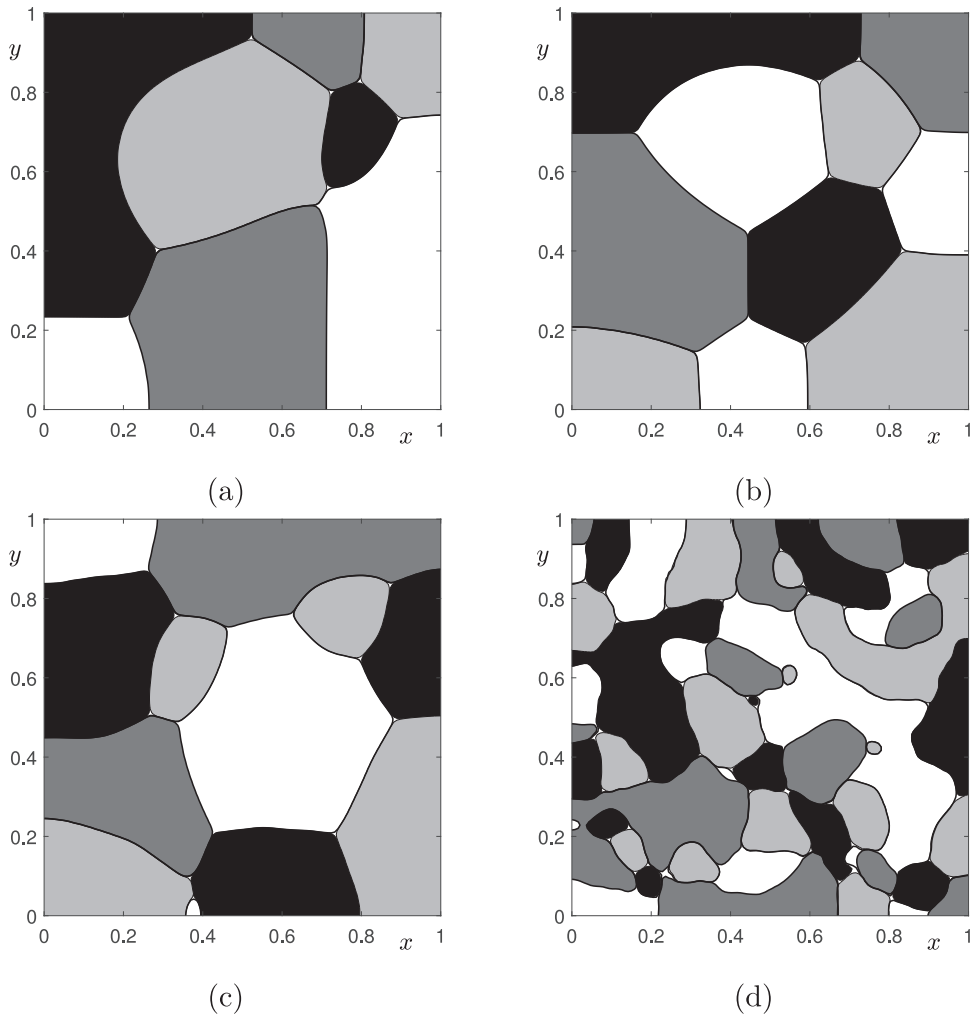


**Fig. 4.** Evolutions of four-component mixture at  $T = 46.875$  with respect to different time steps: (a)  $\Delta t = 0.1h$ , (b)  $\Delta t = h$ , (c)  $\Delta t = 10h$ , and (d)  $\Delta t = 100h$ .

#### 5.4. Convergence test

To numerically show the convergence rates in time and space, we consider the following initial conditions of a three-component system:

$$c_1(x, y, 0) = \frac{1}{3} + 0.01 \cos(3\pi x) + 0.04 \cos(5\pi x), \quad (53)$$

$$c_2(x, y, 0) = \frac{1}{3} + 0.01 \cos(2\pi x) + 0.02 \cos(4\pi x), \quad (54)$$

$$c_3(x, y, 0) = 1 - c_1(x, y, 0) - c_2(x, y, 0). \quad (55)$$

in the domain  $\Omega = (0, 1)^2$ . The parameter  $\epsilon = 0.005$  in this test. To obtain the convergence rate in time, we fix the space step to be  $h = 1/256$ . Because the CH equation does not have analytical solution in general, a reference solution  $c_k^{ref}$  is chosen with very fine time step  $\Delta t^{ref} = 0.1h^2$ . A set of decreasing time step:  $\Delta t = 32\Delta t^{ref}$ ,  $16\Delta t^{ref}$ ,  $8\Delta t^{ref}$ , and  $4\Delta t^{ref}$  is used to perform the numerical simulation until  $T = 0.0183$ . We define the error under a particular time step as the  $l_2$ -norm of the difference between computational result and reference solution at  $t = T$ , i.e.,  $e_{\Delta t} = \|c_{k,ij} - c_{k,ij}^{ref}\|_2$ . The rate of convergence is defined as:  $\log_2 \left( \frac{\|e_{\Delta t}\|_2}{\|e_{\frac{\Delta t}{2}}\|_2} \right)$ . The errors and convergence rates obtained are presented in Table 1. The results indicate that the proposed scheme can achieve second-order accuracy in time.

**Table 1**

Errors and convergence rates with different time steps. Here,  $h = 1/256$  is fixed. The numerical reference is obtained with  $\Delta t^{ref} = 0.1h^2$  at  $t = T = 0.0183$ .

$\Delta t$	$32\Delta t^{ref}$	$16\Delta t^{ref}$	$8\Delta t^{ref}$	$4\Delta t^{ref}$
$c_1: l_2$ -error	7.7291E-4	1.9921E-4	4.9697E-5	1.1868E-5
$c_1$ : Rate		1.96	2.00	2.07
$c_2: l_2$ -error	6.4169E-4	1.6608E-4	4.1477E-5	9.9058E-6
$c_2$ : Rate		1.95	2.00	2.07

**Table 2**

Errors and convergence rates with different space steps. Here,  $\Delta t = 0.0001$  is fixed. The numerical reference is obtained with  $h^{ref} = 1/1024$  at  $t = T = 0.0024$ .

$h$	$64h^{ref}$	$32h^{ref}$	$16h^{ref}$	$8h^{ref}$
$c_1: l_2$ -error	1.9921E-4	5.5238E-5	1.4068E-5	3.4167E-6
$c_1$ : Rate		1.85	1.97	2.04
$c_2: l_2$ -error	2.4660E-4	6.3946E-5	1.5543E-5	3.2783E-6
$c_2$ : Rate		1.95	2.04	2.25

To obtain the convergence rate in space, we fix the time step to be  $\Delta t = 0.0001$ . The reference solution  $c_k^{ref}$  is chosen with very fine space step  $h^{ref} = 1/1024$ . A set of decreasing space step:  $h = 64h^{ref}$ ,  $32h^{ref}$ ,  $16h^{ref}$ , and  $8h^{ref}$  is used to perform the numerical simulation until  $T = 0.0024$ . We define the error under a particular time step as the  $l_2$ -norm of the difference between computational result and reference solution at  $t = T$ , i.e.,

$$e_h = \left\| c_{k,ij} - 0.25 \left( c_{k,2^p i - 2^{p-1}, 2^p j - 2^{p-1}}^{ref} + c_{k,2^p i - 2^{p-1} + 1, 2^p j - 2^{p-1} + 1}^{ref} + c_{k,2^p i - 2^{p-1} + 1, 2^p j - 2^{p-1}}^{ref} + c_{k,2^p i - 2^{p-1}, 2^p j - 2^{p-1} + 1}^{ref} \right) \right\|_2,$$

where  $p = 3, 4, 5$ , and  $6$  with respect to  $h = 8h^{ref}$ ,  $16h^{ref}$ ,  $32h^{ref}$ , and  $64h^{ref}$  respectively. The rate of convergence is defined as:  $\log_2 \left( \frac{\|e_h\|_2}{\|e_{\frac{h}{2}}\|_2} \right)$ . The errors and convergence rates are listed in Table 2. The results indicate that the proposed method can achieve second-order accuracy in space.

5.5. Triple junction

We perform the evolution of triple junction in a four-component system. The initial state in two-dimensional domain  $\Omega = (0, 1)^2$  is illustrated in Fig. 5(a) with the initial angles:  $90^\circ$  and  $180^\circ$  at the interfaces. We use the space step  $h = 1/256$ , time step  $\Delta t = h$ ,  $\epsilon = 0.0019$  to perform the simulation until the solution becomes numerically stationary, i.e.,  $\|c_{k,ij}^{n+1} - c_{k,ij}^n\|_2 \leq 1.0E-5$ . In Fig. 5, we display the temporal evolution of triple junction at  $t = 0$ ,  $5\Delta t$ , and  $50\Delta t$  (stationary state), where the component 1, 2, 3, and 4 are represented by the black, dark gray, gray, and white regions, respectively. Because the total energy functional is symmetric and the interfacial parameter  $\epsilon$  is constant, we observe that the triple junction angles arrive the value  $120^\circ$  at stationary state. Note that a similar result can be found in the previous work of Lee and Kim [39].

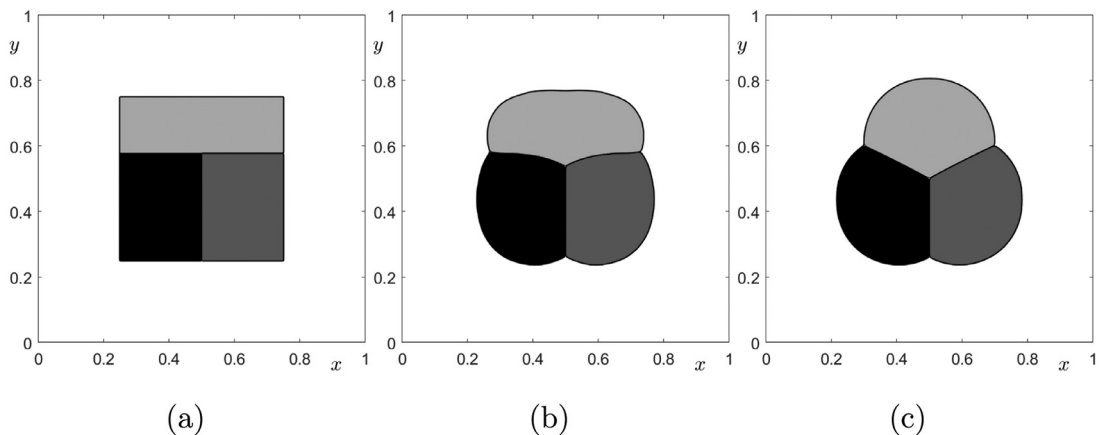


Fig. 5. Temporal evolution of triple junction at (a)  $t = 0$ , (b)  $t = 5\Delta t$ , and (c)  $t = 50\Delta t$ .

### 5.6. Spinodal decomposition

Next, we investigate the effect of initial distribution of phase variables on the phase separation in a quaternary mixture. The computational domain is  $\Omega = (0, 1)^2$ . The following initial conditions are considered:

$$c_1(x, y, 0) = m + 0.05\text{rand}(), \quad (56)$$

$$c_2(x, y, 0) = m + 0.05\text{rand}(), \quad (57)$$

$$c_3(x, y, 0) = m + 0.05\text{rand}(), \quad (58)$$

$$c_4(x, y, 0) = 1 - c_1(x, y, 0) - c_2(x, y, 0) - c_3(x, y, 0), \quad (59)$$

where three different values:  $m = 1/4$ ,  $1/5$ , and  $1/6$  are used. The numerical parameters keep unchanged like those in Section 5.5. The results with  $m = 1/4$  is shown in Fig. 6(a), similar morphologies and evolution dynamics can be observed for four components due to the completely symmetric distribution of initial phase variables. Fig. 6(b) illustrates the results with  $m = 1/5$ . Here, the fourth component (white region) occupies almost half region and the dynamics is similar with the binary system. Fig. 6(c) displays the results with  $m = 1/6$ , where the dynamics of fourth component (white region) is dominant than other components.

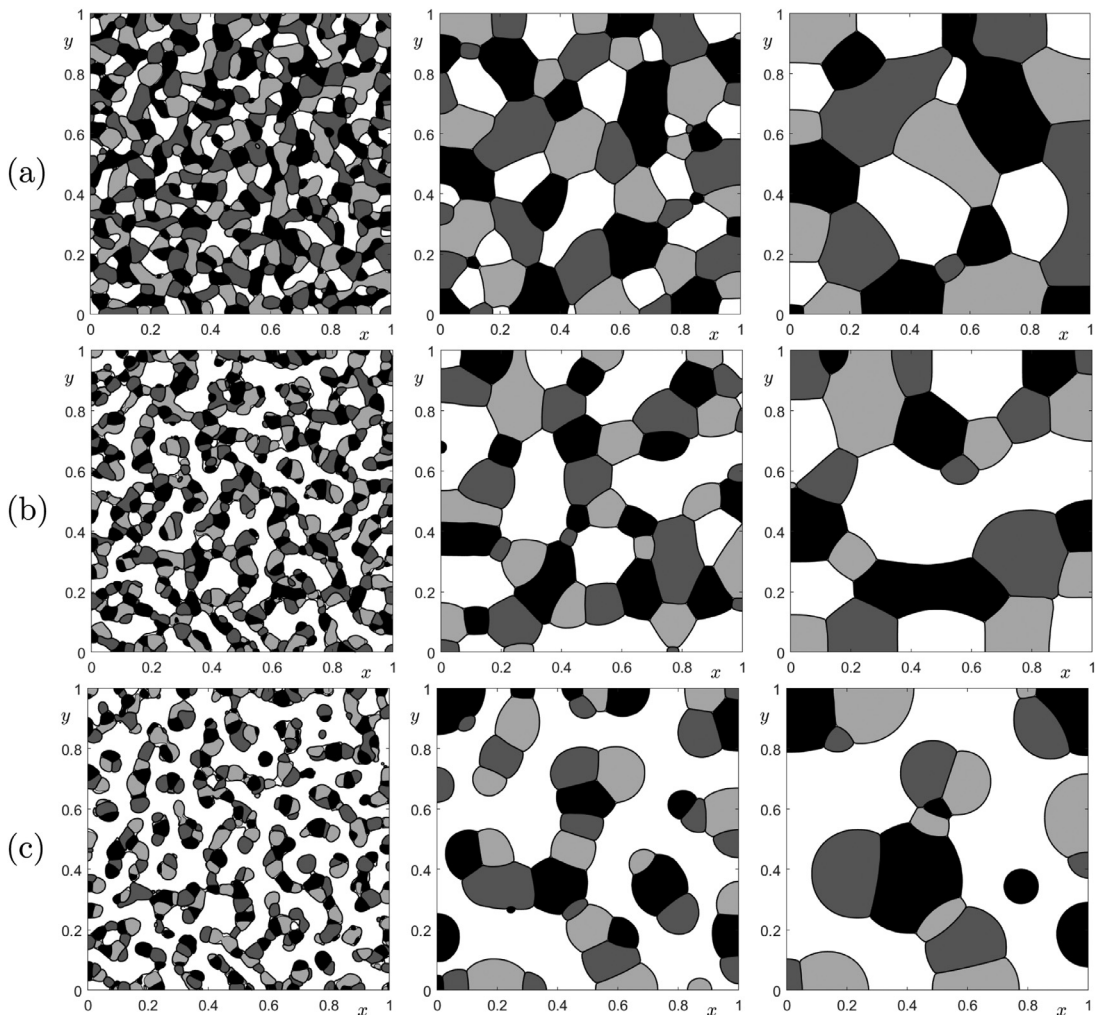


**Fig. 6.** Temporal evolutions of spinodal decomposition with different values: (a)  $m = 1/4$ , (b)  $m = 1/5$ , and (c)  $m = 1/6$ . The computational moment from the left to right in each row are:  $t = \Delta t$ ,  $10\Delta t$ , and  $40\Delta t$ .

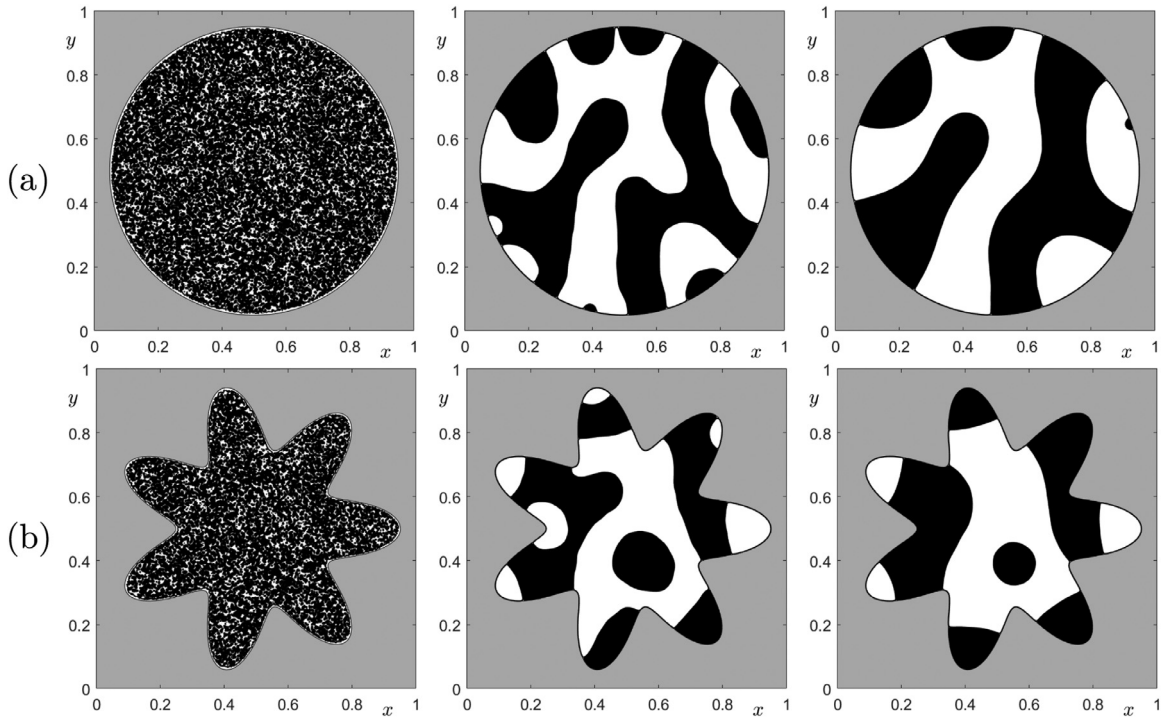


Fig. 7. Temporal evolutions of binary phase separation in complex domains. (a) circle domain, (b) star-shaped domain. The computational moment from the left to right in each row are:  $\Delta t = 0$ ,  $5\Delta t$ , and  $10\Delta t$ .

### 5.7. Binary phase separation in complex domains

One of the practical application of multi-component CH system is to simulate the binary mixture in complex domains. For some details of this application, see [47]. In this model, the complex domain is defined by the initial value of third phase component  $c_3$  and we fix  $c_3$  in the computation. Therefore, this model is very easy to implement without explicit treatment of boundary condition of the complex domain. Here, the modified ternary CH system is defined as follows:

$$\frac{\partial c_1}{\partial t} = \Delta \mu_1, \tag{60}$$

$$\mu_1 = F'(c_1) - \epsilon^2 \Delta c_1 - c_1 c_3 (1 - c_1 - c_3), \tag{61}$$

which is the binary CH equation with a source term. To avoid the bias problem on the domain boundary, we numerically solve  $c_1$  and  $c_2$  alternately. The whole computational domain is  $\Omega = (0, 1)^2$ . The initial values of circle and star-shaped domains are defined as the following Eq. (62) and Eq. (63), respectively:

$$c_3(x, y, 0) = 0.5 + 0.5 \tanh \left( \frac{-0.45 + \sqrt{(x - 0.5)^2 + (y - 0.5)^2}}{2\sqrt{2}\epsilon} \right), \tag{62}$$

$$c_3(x, y, 0) = 0.5 + 0.5 \tanh \left( \frac{-0.35 - 0.1 \cos(7\theta) + \sqrt{(x - 0.5)^2 + (y - 0.5)^2}}{2\sqrt{2}\epsilon} \right), \tag{63}$$

where  $\theta = \tan^{-1}((y - 0.5)/(x - 0.5))$  and  $x \neq 0.5$ . For both cases, the initial condition of  $c_1$  is defined to be  $c_1(x, y, 0) = (1 - c_3(x, y, 0))(0.5 + 0.1\text{rand}())$ , where  $\text{rand}()$  is the random number between  $-1$  and  $1$ . The parameters are:  $h = 1/256$ ,  $\Delta t = h$ ,  $\epsilon = 0.0019$ . The temporal evolutions of binary mixture in circle and star-shaped complex domains are illustrated in Figs. 7(a) and (b), respectively. `plxrunonpara`

### 5.8. Multi-component fluid flows

The multi-component CH system has extensively applications in multi-phase fluid flow simulations, the governing equation is the following dimensionless modified Navier–Stokes–Cahn–Hilliard (NSCH) system:

$$\rho(\mathbf{c}) \left( \frac{\partial \mathbf{u}}{\partial t} + \mathbf{u} \cdot \nabla \mathbf{u} \right) = -\nabla p + \frac{1}{Re} \Delta \mathbf{u} + \frac{\rho(\mathbf{c})}{Fr^2} \mathbf{g} + F_s(\mathbf{c}), \tag{64}$$

$$\nabla \cdot \mathbf{u} = 0, \tag{65}$$

$$\frac{\partial \mathbf{c}}{\partial t} + \nabla \cdot (\mathbf{c}\mathbf{u}) = \frac{1}{Pe} \Delta \mu, \tag{66}$$

$$\mu = F'(\mathbf{c}) - \epsilon^2 \Delta \mathbf{c} + \beta(\mathbf{c}), \tag{67}$$

where  $\rho(\mathbf{c}) = \sum_{k=1}^N \rho_k c_k$  and  $\rho_k$  is the density of  $k$ th fluid component,  $\mathbf{u}$  is the velocity field,  $p$  is the pressure,  $Re$  and  $Fr$  is the Reynolds number and the Froude number,  $\mathbf{g} = (0, -1)$  is the gravitational acceleration, and  $Pe$  is the Peclet number. The surface tension is defined as [48]:

$$F_s(\mathbf{c}) = \sum_{k=1}^{N-1} \left( \sum_{l=k+1}^N 0.5 \frac{1}{We_{kl}} [\mathbf{s}\mathbf{f}(c_k) + \mathbf{s}\mathbf{f}(c_l)] \delta(c_k, c_l) \right), \tag{68}$$

where  $We_{kl}$  is the Weber number between fluid  $k$  and fluid  $l$ ,  $\mathbf{s}\mathbf{f} = -6\sqrt{2}\epsilon^2 \nabla \cdot (\nabla c_k / |\nabla c_k|) |\nabla c_k| \nabla c_k$ , and  $\delta(c_k, c_l) = 5c_k c_l$ . We use the proposed scheme to solve the Eqs. (66) and (67), i.e.,

$$\frac{c_{k,ij}^{n+1} - c_{k,ij}^n}{\Delta t} = \frac{1}{Pe} \Delta_d \mu_{k,ij}^{n+\frac{1}{2}} - \nabla_d \cdot (c_k \mathbf{u})_{ij}^{n+\frac{1}{2}}, \tag{69}$$

$$\begin{aligned} \mu_{k,ij}^{n+\frac{1}{2}} &= \frac{3}{2} (F'(c_{k,ij}^n) - \gamma c_{k,ij}^n) - \frac{1}{2} (F'(c_{k,ij}^{n-1}) - \gamma c_{k,ij}^{n-1}) \\ &\quad + \frac{\gamma}{2} (c_{k,ij}^{n+1} + c_{k,ij}^n) + \frac{\epsilon^2}{2} (\Delta_d c_{k,ij}^{n+1} + \Delta_d c_{k,ij}^n) \\ &\quad + \frac{3}{2} \beta(\mathbf{c}_{ij}^n) - \frac{1}{2} \beta(\mathbf{c}_{ij}^{n-1}), \text{ for } k = 1, 2, \dots, N, \end{aligned} \tag{70}$$

where the half time values  $\mathbf{u}^{n+\frac{1}{2}}$  and  $c_k^{n+\frac{1}{2}}$  are calculated using the second-order extrapolation from previous values, i.e.,  $\mathbf{u}^{n+\frac{1}{2}} \approx (3\mathbf{u}^n - \mathbf{u}^{n-1})/2$  and  $c_k^{n+\frac{1}{2}} \approx (3c_k^n - c_k^{n-1})/2$ . Then, the conservative discretization of convection term is defined as follows [2]:

$$\begin{aligned} \nabla_d \cdot (c_k \mathbf{u})_{ij}^{n+\frac{1}{2}} &= [(c_k u)_x + (c_k v)_y]_{ij}^{n+\frac{1}{2}} \\ &= \frac{u_{i+\frac{1}{2},j}^{n+\frac{1}{2}} (c_{k,i+1,j}^{n+\frac{1}{2}} + c_{k,ij}^{n+\frac{1}{2}}) - u_{i-\frac{1}{2},j}^{n+\frac{1}{2}} (c_{k,ij}^{n+\frac{1}{2}} + c_{k,i-1,j}^{n+\frac{1}{2}})}{2h} \\ &\quad + \frac{v_{i,j+\frac{1}{2}}^{n+\frac{1}{2}} (c_{k,i,j+1}^{n+\frac{1}{2}} + c_{k,ij}^{n+\frac{1}{2}}) - v_{i,j-\frac{1}{2}}^{n+\frac{1}{2}} (c_{k,ij}^{n+\frac{1}{2}} + c_{k,i,j-1}^{n+\frac{1}{2}})}{2h}. \end{aligned} \tag{71}$$

The projection method [2] is used to solve the modified NS Eqs. (64) and (65).

First, we investigate the evolution of five-component Rayleigh–Taylor instability in the domain  $\Omega = (0, 1) \times (0, 4)$  with the mesh size  $64 \times 256$ . The initial conditions of phase variables shown in Fig. 8(a) are defined by a set of cosine functions with amplitude 0.05. The initial velocity field is zero, i.e.,  $\mathbf{u}(x, y, 0) = (u(x, y, 0), v(x, y, 0)) = (0, 0)$ . The surface tension effect is omitted and the following numerical parameters are used:  $\Delta t = 0.002$ ,  $\epsilon = 0.0094$ ,  $Pe = 1/\epsilon$ ,  $Re = 3000$ , and  $Fr = 1$ . The density of component from the top to bottom in initial state is 5, 4, 3, 2, and 1, respectively. The temporal evolution is shown in Figs. 8(a)–(g), we observe that the heavy fluid components fall down and light fluid components raise up.

Then, we consider the rising bubble in a four-component system. The computational domain is  $\Omega = (0, 1) \times (0, 4)$  with mesh size  $64 \times 256$ . The initial conditions are set to be

$$c_1(x, y, 0) = 0.5 + 0.5 \tanh \left( \frac{0.25 - \sqrt{(x - 0.5)^2 + (y - 0.4)^2}}{2\sqrt{2}\epsilon} \right), \tag{72}$$

$$c_2(x, y, 0) = -0.5 - 0.5 \tanh \left( \frac{y - 0.8}{2\sqrt{2}\epsilon} \right) - c_1(x, y, 0), \tag{73}$$

$$c_3(x, y, 0) = 0.5 \tanh \left( \frac{y - 0.8}{2\sqrt{2}\epsilon} \right) - 0.5 \tanh \left( \frac{y - 2.5}{2\sqrt{2}\epsilon} \right), \tag{74}$$

$$c_4(x, y, 0) = 1 - c_1(x, y, 0) - c_2(x, y, 0) - c_3(x, y, 0). \tag{75}$$

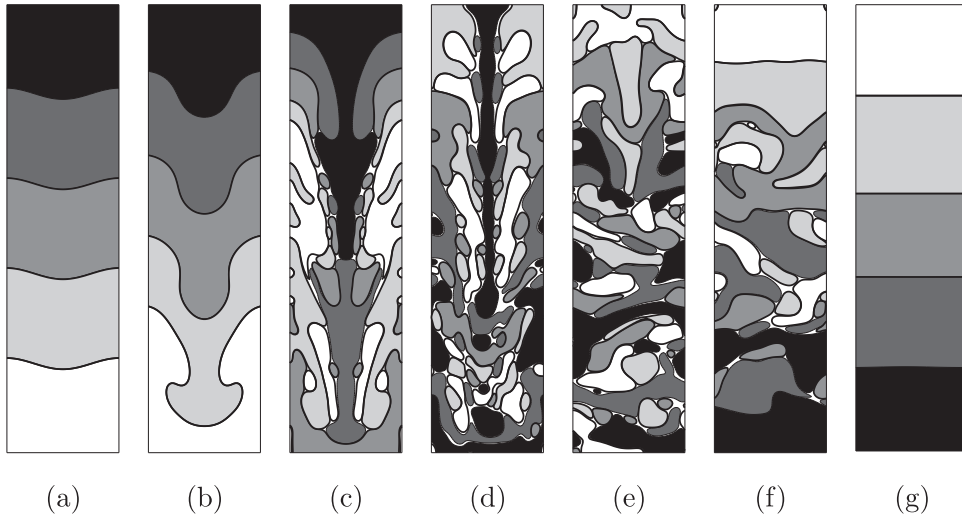


**Fig. 8.** Temporal evolution of five-component Rayleigh-Taylor instability. The computational moments from (a) to (g) are:  $t = 0, 2\Delta t, 4\Delta t, 6\Delta t, 8\Delta t, 20\Delta t,$  and  $100\Delta t$ .

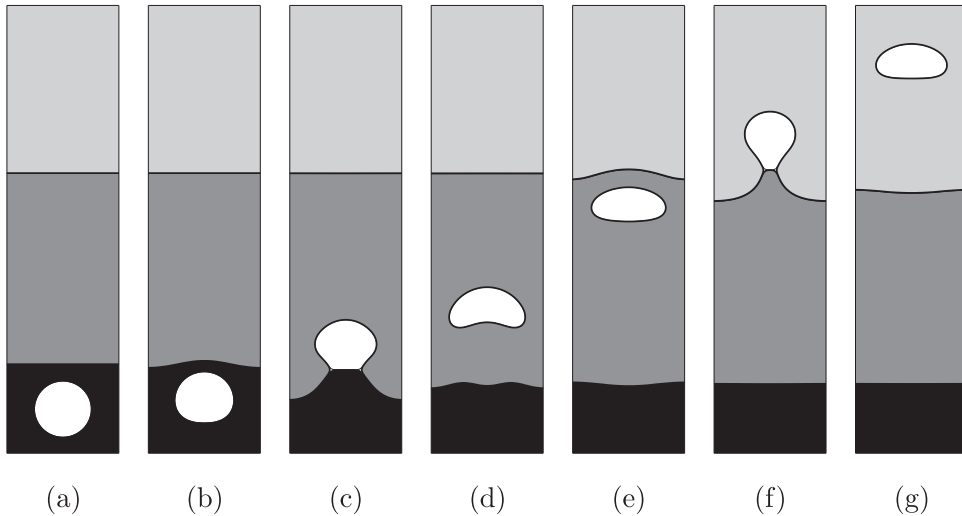


**Fig. 9.** Temporal evolution of rising bubble in a four-component system. The computational moments from (a) to (g) are:  $t = 0, \Delta t, 5\Delta t, 7\Delta t, 14\Delta t, 20\Delta t,$  and  $25\Delta t$ .

Numerical parameters of  $\Delta t = 0.1h$ ,  $\epsilon = 0.006\sqrt{2}$ ,  $Pe = 0.1/\epsilon$ ,  $Re = 100$ ,  $Fr = 1$ ,  $We_{12} = 30$ ,  $We_{13} = 20$ ,  $We_{14} = 40$ ,  $We_{23} = 15$ ,  $We_{24} = 1$ , and  $We_{34} = 60$  are used. The fluid component 1, 2, 3, and 4 are defined in the white, black, dark gray, and gray regions, respectively. We set densities:  $\rho_1 = 1$ ,  $\rho_2 = 4$ ,  $\rho_3 = 3$ , and  $\rho_4 = 2$ . From the results shown in [Figs. 9\(a\)-\(g\)](#), we observe that the light bubble raises and deforms in different fluid components.

## 6. Conclusions

We proposed an unconditionally stable second-order linear scheme for the  $N$ -component CH system. This numerical scheme was derived from the classical second-order CN scheme and adopted the idea of stabilized method, which was unconditionally stable for the whole system. Our scheme was easy to implement because all nonlinear terms were treated as source terms. The nonlinear multigrid algorithm with Gauss-Seidel-type iteration was used to solve the obtained discrete linear system. Various numerical experiments were performed to show that the proposed scheme was accurate, unconditionally stable, and had second-order accuracy in time and space. Moreover, the proposed scheme could be applied to simulate the binary spinodal decomposition in complex domains and multi-phase fluid flows.

## Declaration of Competing Interest

The authors declare that they have no known competing financial interests or personal relationships that could have appeared to influence the work reported in this paper.

## CRediT authorship contribution statement

**Junxiang Yang:** Resources, Writing - original draft, Writing - review & editing, Supervision. **Junseok Kim:** Data curation, Writing - original draft, Writing - review & editing, Supervision.

## Acknowledgments

J. Yang is supported by China Scholarship Council (201908260060). The corresponding author (J.S. Kim) was supported by Basic Science Research Program through the National Research Foundation of Korea (NRF) funded by the Ministry of Education (NRF-2019R1A2C1003053). The authors are grateful to the anonymous referees whose valuable suggestions and comments significantly improved the quality of this paper.

## References

- [1] Cahn JW, Hilliard JE. Free energy of a nonuniform system. i. interfacial free energy. *J Chem Phys* 1958;28:258–67.
- [2] Kim J. Phase-field models for multi-component fluid flows. *Commun Comput Phys* 2012;12(3):613–61.
- [3] Yang X, Yu H. Efficient second order unconditionally stable schemes for a phase field moving contact line model using an invariant energy quadratization approach. *SIAM J Sci Comput* 2018;40(3):889–914.
- [4] Guillén-González F, Tierra G. Unconditionally energy stable numerical schemes for phase-field vesicle membrane model. *J Comput Phys* 2018;354(1):67–85.
- [5] Wise SM, Lowengrub JS, Cristini V. An adaptive multigrid algorithm for simulating solid tumor growth using mixture models. *Math Comput Model* 2011;53(1–2):1–20.
- [6] Wu X, van Zwieten GJ, van der ZKG. Stabilized second-order convex splitting schemes for cahn–hilliard models with application to diffuse-interface tumor-growth models. *Int J Numer Meth Bio* 2014;30(2):180–203.
- [7] Avalos E, Teramoto T, Komiyama H, Yabu H, Nishiura Y. Transformation of block copolymer nanoparticles from ellipsoids with striped lamellae into onionlike spheres and dynamical control via coupled cahn–hilliard equations. *ACS Omega* 2018;3:1304–14.
- [8] Choi Y, Jeong D, Kim J. Curve and surface smoothing using a modified cahn–hilliard equation. *Math Probl Eng* 2017;2017:5971295.
- [9] Myśliński A, Wróblewski M. Structural optimization of contact problems using cahn–hilliard model. *Comput Struct* 2017;180:52–9.
- [10] Kim J, Lee S, Choi Y, Lee SM, Jeong D. Basic principles and practical applications of the cahn–hilliard equation. *Math Probl Eng* 2016;2016:9532608.
- [11] Kim J, Kang K, Lowengrub J. Conservative multigrid methods for cahn–hilliard fluids. *J Comput Phys* 2004;193:511–43.
- [12] Eyre DJ. Unconditionally gradient stable time marching the cahn–hilliard equation. In: Bullard JW, Chen LQ, editors. *Computational and mathematical models of microstructural evolution*, in: MRS proceedings, vol. 529. Cambridge University Press; 1998. p. 39–46.
- [13] Jeong D, Choi Y, Kim J. A benchmark problem for the two- and three-dimensional cahn–hilliard equations. *Commun Nonlinear Sci Numer Simulat* 2018;61:149–59.
- [14] Lee S, Shin J. Energy stable compact scheme for cahn–hilliard equation with periodic boundary condition. *Comput Math Appl* 2019;77:189–98.
- [15] Zhu J, Chen L, Shen J, Tikare V. Coarsening kinetics from a variable mobility cahn–hilliard equation - application of semi-implicit fourier spectral method. *Phys Rev E* 1999;60:3564–72.
- [16] Zhao J, Chen L, Wang H. On power law scaling dynamics for the time-fractional phase field models during coarsening. *Commun Nonlinear Sci Numer Simulat* 2019;70:257–70.
- [17] Chen W, Feng W, Liu Y, Wang C, Wise SM. A second order energy stable scheme for the cahn–hilliard–hele–shaw equations. *Discrete Cont Dyn-B* 2019;24(1):149–82.
- [18] Diegel A.E., Wang C., Wang X., Wise S.M.. Convergence analysis and error estimates for a second order accurate finite element method for the cahn–hilliard–navier–stokes system. *Numeri Math* DOI 10.1007/s00211-017-0887-5.
- [19] Yan Y, Chen W, Wang C, Wise SM. A second-order energy stable BDF numerical scheme for the cahn–hilliard equation. *Commun Comput Phys* 2018;23:572–602.
- [20] Chen W, Wang C, Wang X, Wise SM. Positivity-preserving, energy stable numerical schemes for the cahn–hilliard equation with logarithmic potential. *J Comput Phys X* 2019;3:100031.
- [21] Cheng K, Feng W, Wang C, Wise SM. An energy stable fourth order finite difference scheme for the cahn–hilliard equation. *J Comput Appl Math* 2019;362(15):574–95.
- [22] Cheng K., Wang C., Wise S.M., Yue X.. A second-order, weakly energy-stable pseudo-spectral scheme for the cahn–hilliard equation and is solution by the homogeneous linear iteration method. *J Sci Comput* DOI 10.1007/s10915-016-0228-3.
- [23] Gong Y, Zhao J, Wang Q. Linear second order in time energy stable schemes for hydrodynamic models of binary mixtures based on a spatially pseudospectral approximation. *Adv Comput Math* 2018;44:1573–600.
- [24] Diegel AE, Wang C, Wise SM. Stability and convergence of a second-order mixed finite element method for the cahn–hilliard equation. *IMA J Numer Anal* 2016;36(4):1867–97.
- [25] Brenner SC, Diegel AE, Sung L. A robust solver for a mixed finite element method for the cahn–hilliard equation. *J Comput Appl Math* 2020;364:112322.
- [26] Diegel AE, Feng XH, Wise SM. Analysis of a mixed finite element method for a cahn–hilliard–darcy–stokes system. *SIAM J Numer Anal* 2015;53(1):127–52.
- [27] Weng Z, Zhai S, Feng X. A fourier spectral method for fractional-in-space cahn–hilliard equation. *Appl Math Model* 2017;42:462–77.
- [28] Guillén-González F, Tierra G. On linear schemes for the cahn–hilliard diffuse interface model. *J Comput Phys* 2013;234:140–71.
- [29] Yang X, Zhao J, Wang Q. Numerical approximations for the molecular beam epitaxial growth model based on the invariant energy quadratization method. *J Comput Phys* 2017;333:104–27.
- [30] Shen J, Xu J, Yang J. The scalar auxiliary variable (SAV) approach for gradient flows. *J Comput Phys* 2018;353:407–16.
- [31] Zhu G, Chen H, Yao J, Sun S. Efficient energy-stable schemes for the hydrodynamics coupled phase-field model. *Appl Math Model* 2019;70:82–108.
- [32] Li Y, Kim J, Wang N. An unconditionally energy-stable second-order time-accurate scheme for the cahn–hilliard equation on surfaces. *Commun Nonlinear Sci Numer Simulat* 2017;53:213–27.
- [33] Shin J, Lee HG, Lee JY. Convex splitting runge–kutta methods for phase-field models. *Comput Math Appl* 2017;73(11):2388–403.
- [34] Shin J, Lee HG, Lee JY. Unconditionally stable methods for gradient flow using convex splitting runge–kutta scheme. *J Comput Phys* 2017;347(15):367–81.

- [35] Bhattacharyya S, Abinandanan TA. A study of phase separation in ternary alloys. *Bull Mater Sci* 2003;26:193.
- [36] Yang Z, Dong S. Multiphase flows of  $n$  immiscible incompressible fluids: An outflow/open boundary condition and algorithm. *J Comput Phys* 2018;366(1):33–70.
- [37] Liang H, Xu J, Chen J, Chai Z, Shi B. Lattice boltzmann modeling of wall-bounded ternary fluid flow. *Appl Math Model* 2019;73:487–513.
- [38] Bretin E, Danescu A, Penuelas J, Masnou S. Multiphase mean curvature flows with high mobility contrasts: A phase-field approach, with applications to nanowires. *J Comput Phys* 2018;365(15):324–49.
- [39] Lee HG, Kim J. A second-order accurate non-linear difference scheme for the  $n$ -component cahn–hilliard system. *Physica A* 2008;387:4787–99.
- [40] Lee HG, Choi JW, Kim J. A practically unconditionally gradient stable scheme for the  $n$ -component cahn–hilliard system. *Physica A* 2012;391:1009–19.
- [41] Yang X, Zhao J, Wang Q, Shen J. Numerical approximations for a three components cahn–hilliard phase-field model based on the invariant energy quadratization method. *Math Models Methods Appl Sci* 2017;27(11):1993–2030.
- [42] Trottenberg U, Oosterlee C, Schüller A. *Multigrid*. New York: Academic Press; 2001.
- [43] Shen ZL, Huang TZ, Carpentieri B, Wen C, Gu XM. Block-accelerated aggregation multigrid for markov chains with application to pagerank problems. *Commun Nonlinear Sci Numer Simulat* 2018;59:472–87.
- [44] Shen J, Yang X. Numerical approximations of allen–cahn and cahn–hilliard equations. *Discrete Contin Dyn Syst* 2010;28(4):1669–91.
- [45] Condatte N, Melcher C, Suli E. Spectral approximation of pattern-forming nonlinear evolution equations with double-well potentials of quadratic growth. *Math Comput* 2011;80(273):205–23.
- [46] Nochetto RH, Salgado AJ, Tomas I. A diffuse interface model for two-phase ferrofluid flows. *Comput Methods Appl Mech Engrg* 2016;309(1):497–531.
- [47] Jeong D, Yang J, Kim J. A practical and efficient numerical method for the cahn–hilliard equation in complex domains. *Commun Nonlinear Sci Numer Simulat* 2019;73:217–28.
- [48] Kim J. A generalized continuous surface tension force formulation for phase-field models for multi-component immiscible fluid flows. *Comput Methods Appl Mech Engrg* 2009;198:3105–12.